Chapter 5
Geometric Shapes of Nuclei

In this chapter we shall study nuclear sizes and shapes. In principle, this information may be obtained from scattering experiments (e.g., scattering of protons or α-particles) and when Rutherford discovered that nuclei have a radial extent of less than 10^{-14} m, he employed α-scattering. In practice, however, there are difficulties in extracting detailed information from such experiments. Firstly, these projectiles are themselves extended objects. Therefore, the cross-section reflects not only the structure of the target, but also that of the projectile. Secondly, the nuclear forces between the projectile and the target are complex and not well understood.

Electron scattering is particularly valuable for investigating small objects. As far as we know electrons are point-like objects without any internal structure. The interactions between an electron and a nucleus, nucleon or quark take place via the exchange of a virtual photon – this may be very accurately calculated within quantum electrodynamics (QED). These processes are in fact manifestations of the well known electromagnetic interaction, whose coupling constant $\alpha \approx 1/137$ is much less than one. This means that higher order corrections play only a tiny role.

5.1 Kinematics of Electron Scattering

In electron scattering experiments one employs highly relativistic particles. Hence it is advisable to use four-vectors in kinematical calculations. The zero component of space-time four-vectors is time, the zero component of four-momentum vectors is energy:

$$\begin{aligned} x &= (x_0, x_1, x_2, x_3) \quad = (ct, \boldsymbol{x}) \,, \\ p &= (p_0, p_1, p_2, p_3) = (E/c, \boldsymbol{p}) \,. \end{aligned} \tag{5.1}$$

B. Povh et al., *Particles and Nuclei*, Graduate Texts in Physics,
DOI 10.1007/978-3-662-46321-5_5

Three-vectors are designated by bold-faced type to distinguish them from four-vectors. The Lorentz-invariant scalar product of two four-vectors a and b is defined by

$$a \cdot b \;=\; a_0 b_0 - a_1 b_1 - a_2 b_2 - a_3 b_3 \;=\; a_0 b_0 - \boldsymbol{a} \cdot \boldsymbol{b} \,. \tag{5.2}$$

In particular, this applies to the four-momentum squared:

$$p^2 = \frac{E^2}{c^2} - \boldsymbol{p}^2 \,. \tag{5.3}$$

This squared product is equal to the square of the rest mass m (multiplied by c^2). This is so since a reference frame in which the particle is at rest can always be found and there $\boldsymbol{p} = 0$, and $E = mc^2$. The quantity

$$m = \sqrt{p^2}\,/c \tag{5.4}$$

is called the *invariant mass*. From (5.3) and (5.4) we obtain the relativistic energy-momentum relation

$$E^2 - \boldsymbol{p}^2 c^2 = m^2 c^4 \tag{5.5}$$

and thus

$$E \approx |\boldsymbol{p}|\, c \qquad \text{if} \quad E \gg mc^2 \,. \tag{5.6}$$

For electrons, this approximation is already valid at energies of a few MeV.

■ Consider the scattering of an electron with four-momentum p off a particle with four-momentum P (Fig. 5.1). Energy and momentum conservation imply that the sums of the four-momenta before and after the reaction are identical:

$$p + P = p' + P' \,, \tag{5.7}$$

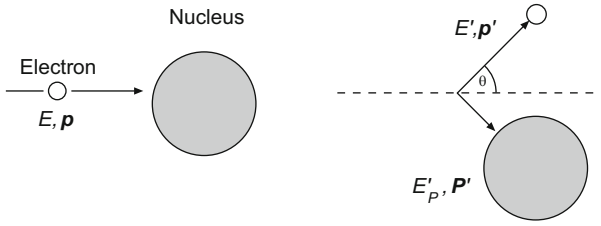

Fig. 5.1 Kinematics of elastic electron-nucleus scattering

or squared:

$$p^2 + 2pP + P^2 = p'^2 + 2p'P' + P'^2 \,. \tag{5.8}$$

In elastic scattering the invariant masses m_e and M of the colliding particles are unchanged. Hence from

$$p^2 = p'^2 = m_e^2 c^2 \qquad \text{and} \qquad P^2 = P'^2 = M^2 c^2 \tag{5.9}$$

it follows that

$$p \cdot P \;=\; p' \cdot P' \,. \tag{5.10}$$

Usually only the scattered electron is detected and not the recoiling particle. In this case the relation

$$p \cdot P \;=\; p' \cdot (p + P - p') \;=\; p'p + p'P - m_e^2 c^2 \tag{5.11}$$

is used. Consider the laboratory frame where the particle with four-momentum P is at rest before the collision. Then the four-momenta can be written as

$$p = (E/c, \boldsymbol{p}) \quad p' = (E'/c, \boldsymbol{p}') \quad P = (Mc, \boldsymbol{0}) \quad P' = (E'_P/c, \boldsymbol{P}') \,. \tag{5.12}$$

Hence (5.11) yields

$$E \cdot Mc^2 = E'E - \boldsymbol{p}\boldsymbol{p}'c^2 + E'Mc^2 - m_e^2 c^4 \,. \tag{5.13}$$

At high energies, $m_e^2 c^4$ may be neglected and $E \approx |\boldsymbol{p}| \cdot c$ (Eq. (5.6)) can be safely used. One thus obtains a relation between the angle and the energy

$$E \cdot Mc^2 = E'E \cdot (1 - \cos\theta) + E' \cdot Mc^2 \,. \tag{5.14}$$

In the laboratory system, the energy E' of the scattered electron is

$$E' = \frac{E}{1 + E/Mc^2 \cdot (1 - \cos\theta)} \,. \tag{5.15}$$

The angle θ through which the electron is deflected is called the *scattering angle*. The recoil which is transferred to the target is given by the difference $E - E'$. In elastic scattering, a one-to-one relationship (5.15) exists between the scattering angle θ and the energy E' of the scattered electron; (5.15) does not hold for inelastic scattering.

The angular dependence of the scattering energy E' is described by the term $(1 - \cos\theta)$ multiplied by E/Mc^2. Hence the recoil energy of the target increases with the ratio of the relativistic electron mass E/c^2 to the target mass M. This is in accordance with the classical laws of collision.

In electron scattering at the relatively low energy of 0.5 GeV off a nucleus with mass number $A = 50$ the scattering energy varies by only 2 % between forward and backward scattering. The situation is very different for 10 GeV-electrons scattering

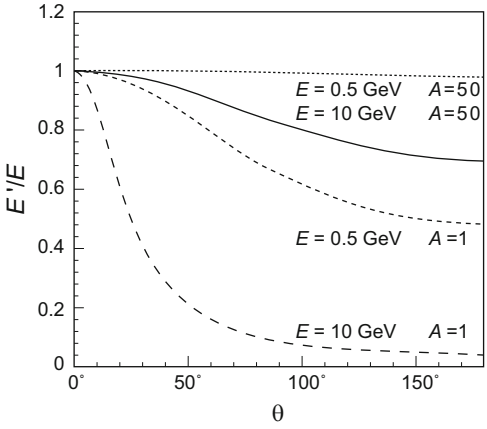

Fig. 5.2 Angular dependence of the scattering energy of electrons normalised to beam energy, E'/E, in elastic electron-nucleus scattering. The curves show this dependence for two different beam energies (0.5 and 10 GeV) and for two nuclei with different masses ($A = 1$ and $A = 50$)

off protons. The scattering energy E' then varies between 10 GeV ($\theta \approx 0°$) and 445 MeV ($\theta = 180°$) (cf. Fig. 5.2).

5.2 The Rutherford Cross-Section

We will now consider the cross-section for an electron with energy E scattering off an atomic nucleus with charge Ze. For the calculation of the reaction kinematics to be sufficiently precise, it must be both relativistic and quantum mechanical. We will approach this goal step by step. Firstly, we introduce the Rutherford scattering formula. By definition, this formula yields the cross-section up to spin effects. For heavy nuclei and low energy electrons, the recoil can, from (5.15), be neglected. In this case, the energy E and the modulus of the momentum $\boldsymbol{p}$ are the same before and after the scattering. The kinematics can be calculated in the same way as, for example, the hyperbolic trajectory of a comet which is deflected by the Sun as it traverses the solar system. As long as the radius of the scattering centre (nucleus, Sun) is smaller than the closest approach of the projectile (electron, comet) then the spatial extension of the scattering centre does not affect this purely classical calculation. This leads to the Rutherford formula for the scattering of a particle with charge ze and kinetical energy E_{kin} on a target nucleus with charge Ze:

$$\left(\frac{\mathrm{d}\sigma}{\mathrm{d}\Omega}\right)_{\text{Rutherford}} = \frac{(zZe^2)^2}{(4\pi\varepsilon_0)^2 \cdot (4E_{\text{kin}})^2 \sin^4 \frac{\theta}{2}} \,. \tag{5.16}$$

Exactly the same equation is obtained by a calculation of this cross-section in non-relativistic quantum mechanics using Fermi's golden rule. This we will now demonstrate. To avoid unnecessary repetitions we will consider the case of a central charge with finite spatial distribution.

Scattering off an extended charge distribution Consider the case of a target so heavy that the recoil is negligible. We can then use three-momenta. If Ze is small, i.e., if

$$Z\alpha \ll 1 \,, \tag{5.17}$$

the *Born approximation* can be applied, and the wave functions ψ_i and ψ_f of the incoming and of the outgoing electron can be described by plane waves

$$\psi_i = \frac{1}{\sqrt{V}}\, \mathrm{e}^{i\boldsymbol{p}\boldsymbol{x}/\hbar} \qquad \psi_f = \frac{1}{\sqrt{V}}\, \mathrm{e}^{i\boldsymbol{p}'\boldsymbol{x}/\hbar} \,. \tag{5.18}$$

We can sidestep any difficulties related to the normalisation of the wave functions by considering only a finite volume V. We need this volume to be large compared to the scattering centre, and also large enough that the discrete energy states in this volume can be approximated by a continuum. The physical results have, of course, to be independent of V.

We consider an electron beam with a density of n_a particles per unit volume. With the volume of integration chosen to be sufficiently large, the normalisation condition is given by

$$\int_V |\psi_i|^2 \,\mathrm{d}V = n_\mathrm{a} \cdot V \qquad \text{where} \quad V = \frac{N_\mathrm{a}}{n_\mathrm{a}} \,, \tag{5.19}$$

i.e., V is the normalisation volume that must be chosen for a single beam particle.

According to (4.20), the reaction rate W is given by the product of the cross-section σ and the beam particle velocity v_a divided by the above volume. When applying the golden rule (4.19), we get

$$\frac{\sigma v_\mathrm{a}}{V} = W = \frac{2\pi}{\hbar} \left|\langle \psi_f | \mathcal{H}_\mathrm{int} | \psi_i \rangle\right|^2 \frac{\mathrm{d}n}{\mathrm{d}E_f} \,. \tag{5.20}$$

Here, E_f is the total energy (kinetic energy and rest mass) of the final state. Since we neglect the recoil and since the rest mass is a constant, $\mathrm{d}E_f = \mathrm{d}E' = \mathrm{d}E$.

The density n of possible final states in phase space (cf. (4.16)) is

$$\mathrm{d}n(|\boldsymbol{p}'|) = \frac{4\pi |\boldsymbol{p}'|^2 \mathrm{d}|\boldsymbol{p}'| \cdot V}{(2\pi\hbar)^3} \,. \tag{5.21}$$

Therefore the cross-section for the scattering of an electron into a solid angle element $\mathrm{d}\Omega$ is

$$\mathrm{d}\sigma \cdot v_\mathrm{a} \cdot \frac{1}{V} = \frac{2\pi}{\hbar} \left|\langle \psi_f | \mathcal{H}_\mathrm{int} | \psi_i \rangle\right|^2 \frac{V |\boldsymbol{p}'|^2 \mathrm{d}|\boldsymbol{p}'|}{(2\pi\hbar)^3 \mathrm{d}E_f} \,\mathrm{d}\Omega \,. \tag{5.22}$$

The velocity v_a can be replaced, to a good approximation, by the velocity of light c. For large electron energies, $|\boldsymbol{p}'| \approx E'/c$ applies, and we obtain

$$\frac{\mathrm{d}\sigma}{\mathrm{d}\Omega} = \frac{V^2 E'^2}{(2\pi)^2(\hbar c)^4} \left|\langle\psi_f|\mathcal{H}_{\mathrm{int}}|\psi_i\rangle\right|^2 . \tag{5.23}$$

The interaction operator for a charge e in an electric potential ϕ is $\mathcal{H}_{\mathrm{int}} = e\phi$. Hence, the matrix element is

$$\langle\psi_f|\mathcal{H}_{\mathrm{int}}|\psi_i\rangle = \frac{e}{V}\int \mathrm{e}^{-i\boldsymbol{p}'\boldsymbol{x}/\hbar}\,\phi(\boldsymbol{x})\,\mathrm{e}^{i\boldsymbol{p}\boldsymbol{x}/\hbar}\mathrm{d}^3x\,. \tag{5.24}$$

Defining the *momentum transfer* $\boldsymbol{q}$ by

$$\boldsymbol{q} = \boldsymbol{p} - \boldsymbol{p}'\,, \tag{5.25}$$

we may re-write the matrix element as

$$\langle\psi_f|\mathcal{H}_{\mathrm{int}}|\psi_i\rangle = \frac{e}{V}\int \phi(\boldsymbol{x})\,\mathrm{e}^{i\boldsymbol{q}\boldsymbol{x}/\hbar}\,\mathrm{d}^3x\,. \tag{5.26}$$

■ Green's theorem permits us to use a clever trick here: for two arbitrarily chosen scalar fields u and v, which fall off fast enough at large distances, the following equation holds for a sufficiently large integration volume:

$$\int (u\Delta v - v\Delta u)\,\mathrm{d}^3x = 0\,, \qquad \text{with} \quad \Delta = \nabla^2\,. \tag{5.27}$$

Inserting

$$\mathrm{e}^{i\boldsymbol{q}\boldsymbol{x}/\hbar} = \frac{-\hbar^2}{|\boldsymbol{q}|^2}\cdot\Delta\mathrm{e}^{i\boldsymbol{q}\boldsymbol{x}/\hbar} \tag{5.28}$$

into (5.26), we may rewrite the matrix element as

$$\langle\psi_f|\mathcal{H}_{\mathrm{int}}|\psi_i\rangle = \frac{-e\hbar^2}{V|\boldsymbol{q}|^2}\int \Delta\phi(\boldsymbol{x})\,\mathrm{e}^{i\boldsymbol{q}\boldsymbol{x}/\hbar}\,\mathrm{d}^3x\,. \tag{5.29}$$

The potential $\phi(\boldsymbol{x})$ and the charge density $\varrho(\boldsymbol{x})$ are related by Poisson's equation

$$\Delta\phi(\boldsymbol{x}) = \frac{-\varrho(\boldsymbol{x})}{\varepsilon_0}\,. \tag{5.30}$$

In the following, we will assume the charge density $\varrho(\boldsymbol{x})$ to be static, i.e. independent of time.

We now define a charge distribution function f by $\varrho(\boldsymbol{x}) = Zef(\boldsymbol{x})$ which satisfies the normalisation condition $\int f(\boldsymbol{x})\,\mathrm{d}^3x = 1$, and re-write the matrix element as

$$\begin{aligned}\langle\psi_f|\mathcal{H}_{\mathrm{int}}|\psi_i\rangle &= \frac{e\hbar^2}{\varepsilon_0 \cdot V|\boldsymbol{q}|^2}\int \varrho(\boldsymbol{x})\,\mathrm{e}^{i\boldsymbol{q}\boldsymbol{x}/\hbar}\mathrm{d}^3x \\ &= \frac{Z\cdot 4\pi\alpha\hbar^3 c}{|\boldsymbol{q}|^2\cdot V}\int f(\boldsymbol{x})\,\mathrm{e}^{i\boldsymbol{q}\boldsymbol{x}/\hbar}\mathrm{d}^3x\,. \end{aligned} \tag{5.31}$$

The integral

$$F(\boldsymbol{q}) = \int \mathrm{e}^{i\boldsymbol{q}\boldsymbol{x}/\hbar} f(\boldsymbol{x})\mathrm{d}^3x \tag{5.32}$$

is the Fourier transform of the charge function $f(\boldsymbol{x})$, normalised to the total charge. It is called the *form factor* of the charge distribution. The form factor contains all the information about the spatial distribution of the charge of the object being studied. We will discuss form factors and their meaning in the following chapters in some detail.

To calculate the Rutherford cross-section we, by definition, neglect the spatial extension – i.e., we replace the charge distribution by a δ-function. Hence, the form factor is fixed to unity. By inserting the matrix element into (5.23) we obtain

$$\left(\frac{\mathrm{d}\sigma}{\mathrm{d}\Omega}\right)_{\mathrm{Rutherford}} = \frac{4Z^2\alpha^2(\hbar c)^2E'^2}{|\boldsymbol{q}c|^4}\,. \tag{5.33}$$

The $1/\boldsymbol{q}^4$-dependence of the electromagnetic cross-section implies very low event rates for electron scattering with large momentum transfers. The event rates drop off so sharply that small measurement errors in $\boldsymbol{q}$ can significantly falsify the results.

■ Since recoil is neglected in Rutherford scattering, the electron energy and the magnitude of its momentum do not change in the interaction:

$$E = E'\,, \qquad |\boldsymbol{p}| = |\boldsymbol{p}'|\,. \tag{5.34}$$

The magnitude of the momentum transfer $\boldsymbol{q}$ is therefore

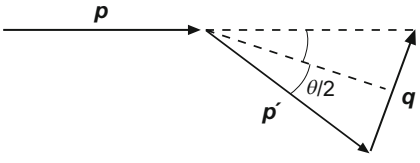

$$|\boldsymbol{q}| = 2\cdot|\boldsymbol{p}|\sin\frac{\theta}{2}\,. \tag{5.35}$$

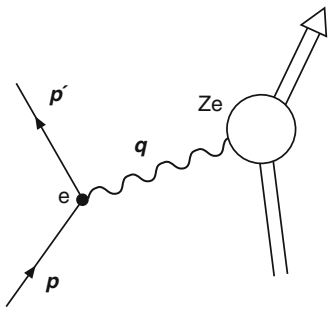

Fig. 5.3 Sketch of elastic electron scattering off a nucleus with charge Z · e

If we recall that $E = |\boldsymbol{p}| \cdot c$ is a good approximation we obtain the relativistic Rutherford scattering formula

$$\left(\frac{\mathrm{d}\sigma}{\mathrm{d}\Omega}\right)_{\text{Rutherford}} = \frac{Z^2\alpha^2(\hbar c)^2}{4E^2 \sin^4 \frac{\theta}{2}} \,. \tag{5.36}$$

The classical Rutherford formula (5.16) may be obtained from (5.33) by applying non-relativistic kinematics: $\boldsymbol{p} = m\boldsymbol{v}$, $E_{\text{kin}} = m\boldsymbol{v}^2/2$ and $E' \approx mc^2$.

Field-theoretical considerations Figure 5.3 is a pictorial representation of a scattering process. In the language of field theory, the electromagnetic interaction of an electron with the charge distribution is mediated by the exchange of a photon, the field quantum of this interaction. The photon which does not itself carry any charge, couples to the charges of the two interacting particles. In the transition matrix element, this yields a factor $Ze \cdot e$ and in the cross-section we have a term $(Ze^2)^2$. The three-momentum transfer $\boldsymbol{q}$ defined in (5.25) is the momentum transferred by the exchanged photon. Hence the reduced de Broglie wavelength of the photon is

$$\lambda\!\!\!^{-} = \frac{\hbar}{|\boldsymbol{q}|} = \frac{\hbar}{|\boldsymbol{p}|} \cdot \frac{1}{2 \sin \frac{\theta}{2}} \,. \tag{5.37}$$

If $\lambda\!\!\!^{-}$ is considerably larger than the spatial extent of the target particle, internal structures cannot be resolved, and the target particle may be considered to be point-like. The Rutherford cross-section from (5.33) was obtained for this case.

In the form (5.33), the dependence of the cross-section on the momentum transfer is clearly expressed. To lowest order the interaction is mediated by the exchange of a single photon. Since the photon is massless, the propagator (4.23) in the matrix element is $1/Q^2$, or $1/|\boldsymbol{q}|^2$ in a non-relativistic approximation. The propagator enters the cross-section squared which leads to the characteristic fast $1/|\boldsymbol{q}|^4$ fall-off of the cross-section.

If the Born approximation condition (5.17) no longer holds, then our simple picture must be modified. Higher order corrections (exchange of several photons) must be included and more complicated calculations (phase shift analyses) are necessary.

5.3 The Mott Cross-Section

Up to now we have neglected the spins of the electron and of the target. At relativistic energies, however, the Rutherford cross-section is modified by spin effects. The *Mott cross-section*, which describes electron scattering and includes effects due to the electron spin, may be written as

$$\left(\frac{\mathrm{d}\sigma}{\mathrm{d}\Omega}\right)^{*}_{\text{Mott}} = \left(\frac{\mathrm{d}\sigma}{\mathrm{d}\Omega}\right)_{\text{Rutherford}} \cdot \left(1 - \beta^2 \sin^2\frac{\theta}{2}\right), \quad \text{with } \beta = \frac{v}{c}. \tag{5.38}$$

The asterisk indicates that the recoil of the nucleus has been neglected in deriving this equation. The expression shows that, at relativistic energies, the Mott cross-section drops off more rapidly at large scattering angles than does the Rutherford cross-section. In the limiting case of $\beta \to 1$, and using $\sin^2 x + \cos^2 x = 1$, the Mott cross-section can be written in a simpler form:

$$\left(\frac{\mathrm{d}\sigma}{\mathrm{d}\Omega}\right)^{*}_{\text{Mott}} = \left(\frac{\mathrm{d}\sigma}{\mathrm{d}\Omega}\right)_{\text{Rutherford}} \cdot \cos^2\frac{\theta}{2} = \frac{4Z^2\alpha^2(\hbar c)^2 E'^2}{|\boldsymbol{q}c|^4}\cos^2\frac{\theta}{2}. \tag{5.39}$$

The additional factor in (5.38) can be understood by considering the extreme case of scattering through 180°. For relativistic particles in the limit $\beta \to 1$, the projection of their spin $\boldsymbol{s}$ on the direction of their motion $\boldsymbol{p}/|\boldsymbol{p}|$ is a conserved quantity. This conservation law follows from the solution of the Dirac equation in relativistic quantum mechanics [3]. It is usually called conservation of *helicity* rather than conservation of the projection of the spin. Helicity is defined by

$$h = \frac{\boldsymbol{s}\cdot\boldsymbol{p}}{|\boldsymbol{s}|\cdot|\boldsymbol{p}|}. \tag{5.40}$$

Particles with spin pointing in the direction of their motion have helicity $+1$, particles with spin pointing in the opposite direction have helicity -1.

Figure 5.4 shows the kinematics of scattering through 180°. We here choose the momentum direction of the incoming electron as the axis of quantisation z. Because of conservation of helicity, the projection of the spin on the z-axis would have to turn over (spin-flip). This, however, is impossible with a spinless target, because of conservation of total angular momentum. The orbital angular momentum $\boldsymbol{L}$ is perpendicular to the direction of motion z. It therefore cannot cause any change in the z-component of the angular momentum. Hence in the limiting case $\beta \to 1$, scattering through 180° must be completely suppressed.

If the target has spin, the spin projection of the electron can be changed, as conservation of angular momentum can be compensated by a change in the spin direction of the target. In this case, the above reasoning is not valid, and scattering through 180° is possible.

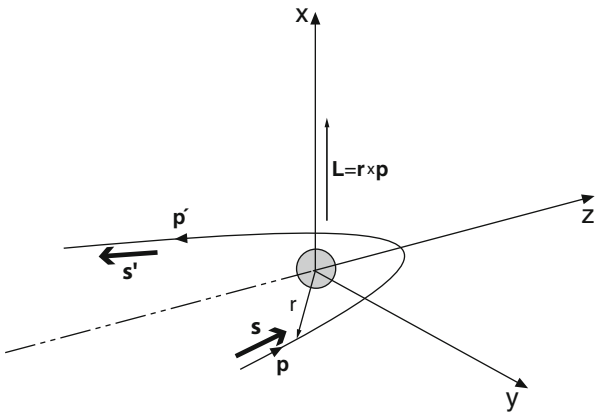

Fig. 5.4 Helicity, $h = \boldsymbol{s} \cdot \boldsymbol{p}/(|\boldsymbol{s}| \cdot |\boldsymbol{p}|)$, is conserved in the $\beta \to 1$ limit. This means that the spin projection on the z-axis would have to change its sign in scattering through 180°. This is impossible if the target is spinless, because of conservation of angular momentum

5.4 Nuclear Form Factors

In actual scattering experiments with nuclei or nucleons, we see that the Mott cross-sections agree with the experimental cross-sections only in the limit $|\boldsymbol{q}| \to 0$. At larger values of $|\boldsymbol{q}|$, the experimental cross-sections are systematically smaller. The reason for this lies in the spatial extension of nuclei and nucleons. At larger values of $|\boldsymbol{q}|$, the reduced wavelength of the virtual photon decreases (5.37), and the resolution increases. The scattered electron no longer sees the total charge, but only parts of it. Therefore, the cross-section decreases.

As we have seen, the spatial extension of a nucleus is described by a form factor (5.32). In the following, we will restrict the discussion to the form factors of spherically symmetric systems which have no preferred orientation in space. In this case, the form factor only depends on the momentum transfer $\boldsymbol{q}$. We symbolise this fact by writing the form factor as $F(\boldsymbol{q}^2)$.

Experimentally, the magnitude of the form factor is determined by the ratio of the measured cross-section to the Mott cross-section

$$\left(\frac{\mathrm{d}\sigma}{\mathrm{d}\Omega}\right)_{\text{exp.}} = \left(\frac{\mathrm{d}\sigma}{\mathrm{d}\Omega}\right)^{*}_{\text{Mott}} \cdot \left|F(\boldsymbol{q}^2)\right|^2 \,. \tag{5.41}$$

One therefore measures the cross-section for a fixed beam energy at various angles (and thus different values of $|\boldsymbol{q}|$) and divides by the calculated Mott cross-section.

In Fig. 5.5, a typical experimental set-up for the measurement of form factors is depicted. The electron beam is provided by a linear accelerator and is directed at a thin target. The scattered electrons are measured in a magnetic spectrometer. In an

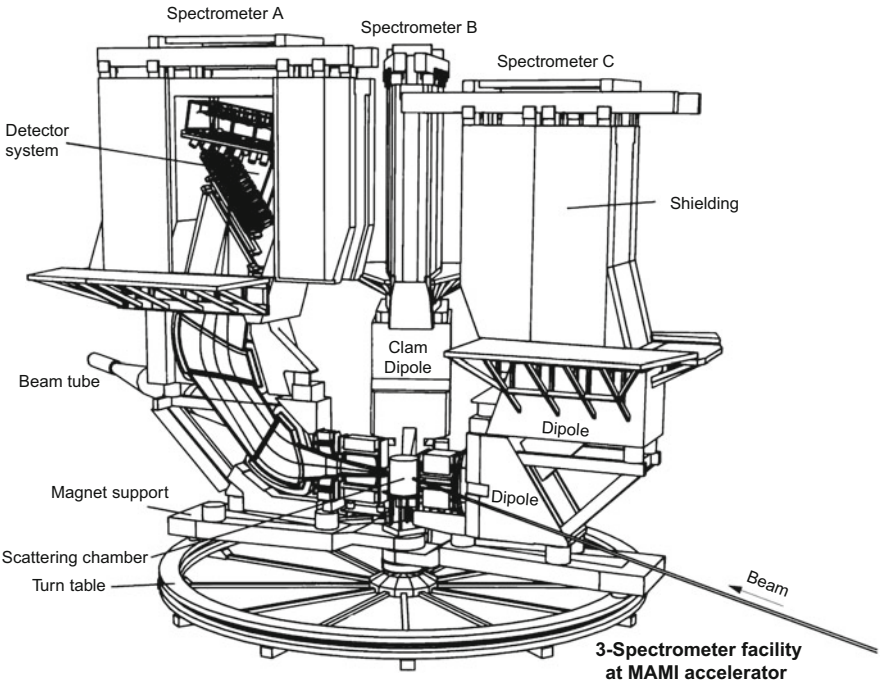

Fig. 5.5 Experimental set-up for the measurement of electron scattering off protons and nuclei at the electron accelerator MAMI-B (Mainzer Microtron). The maximum energy available is 820 MeV. The figure shows three magnetic spectrometers. They can be used individually to detect elastic scattering or in coincidence for a detailed study of inelastic channels. Spectrometer A is shown in cutaway view. The scattered electrons are analysed according to their momentum by two dipole magnets supplemented by a system of detectors made up of wire chambers and scintillation counters. The diameter of the rotating ring is approximately 12 m (Courtesy of Arnd P. Liesenfeld (Mainz), who produced this picture)

analysing magnet the electrons are deflected according to their momentum, and are then detected in wire chambers. The spectrometer can be rotated around the target in order to allow measurements at different angles θ.

Examples of form factors The first measurements of nuclear form factors were carried out in the early 1950s at a linear accelerator at Stanford University, California. Cross-sections were measured for a large variety of nuclei at electron energies of about 500 MeV.

An example of one of the first measurements of form factors can be seen in Fig. 5.6. It shows the ^{12}C cross-section measured as a function of the scattering angle θ. The fast fall-off of the cross-section at large angles corresponds to the $1/|\boldsymbol{q}|^4$-dependence. Superimposed is a typical diffraction pattern associated with the form factor. It has a minimum at $\theta \approx 51°$ or $|\boldsymbol{q}|/\hbar \approx 1.8\,\mathrm{fm}^{-1}$. We want to now

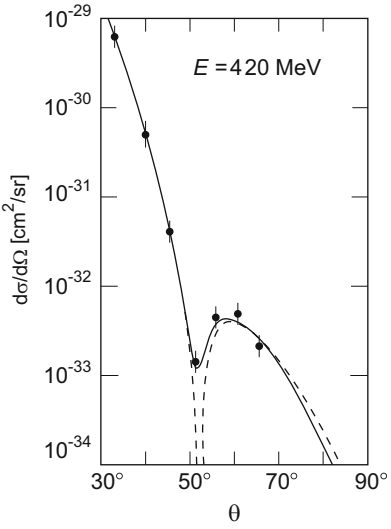

Fig. 5.6 Measurement of the form factor of ^{12}C by electron scattering (From [4]). The figure shows the differential cross-section measured at a fixed beam energy of 420 MeV, at 7 different scattering angles. The *dashed line* corresponds to scattering of a plane wave off an homogeneous sphere with a diffuse surface (Born approximation). The *solid line* corresponds to an exact phase shift analysis which was fitted to the experimental data

discuss this figure and describe what information about the nucleus can be extracted from it.

As we have seen, the form factor $F(\boldsymbol{q}^2)$ is under certain conditions (negligible recoil, Born approximation) the Fourier transform of the charge distribution $f(\boldsymbol{x})$

$$F(\boldsymbol{q}^2) = \int \mathrm{e}^{i\boldsymbol{q}\boldsymbol{x}/\hbar} f(\boldsymbol{x})\, \mathrm{d}^3x\,. \tag{5.42}$$

For spherically symmetric cases f only depends upon the radius $r = |\boldsymbol{x}|$. Integration over the total solid angle then yields

$$F(\boldsymbol{q}^2) = 4\pi \int f(r)\, \frac{\sin |\boldsymbol{q}| r/\hbar}{|\boldsymbol{q}| r/\hbar}\, r^2\, \mathrm{d}r\,, \tag{5.43}$$

with the normalisation

$$1 = \int f(\boldsymbol{x})\, \mathrm{d}^3x = \int_0^\infty \int_{-1}^{+1} \int_0^{2\pi} f(r)\, r^2\, \mathrm{d}\phi\, \mathrm{d}\cos\vartheta\, \mathrm{d}r = 4\pi \int_0^\infty f(r)\, r^2\, \mathrm{d}r\,. \tag{5.44}$$

Table 5.1 Connection between charge distributions and form factors for some spherically symmetric charge distributions in Born approximation

Charge distribution $f(r)$		Form factor $F(\boldsymbol{q}^2)$	
Point	$\delta(r)/4\pi$	1	Constant
Exponential	$(a^3/8\pi)\cdot\exp(-ar)$	$\left(1+\boldsymbol{q}^2/a^2\hbar^2\right)^{-2}$	Dipole
Gaussian	$\left(a^2/2\pi\right)^{3/2}\cdot\exp\left(-a^2r^2/2\right)$	$\exp\left(-\boldsymbol{q}^2/2a^2\hbar^2\right)$	Gaussian
Homogeneous sphere	$\begin{cases} 3/4\pi R^3 & \text{for } r\le R \\ 0 & \text{for } r>R \end{cases}$	$3\,\alpha^{-3}\,(\sin\alpha-\alpha\cos\alpha)$ with $\alpha=\lvert\boldsymbol{q}\rvert R/\hbar$	Oscillating

In principle, the radial charge distribution could be determined from the inverse Fourier transform, using the $\boldsymbol{q}^2$-dependence of the experimental form factor

$$f(r)=\frac{1}{(2\pi)^3}\int F(\boldsymbol{q}^2)\,\mathrm{e}^{-i\boldsymbol{q}\boldsymbol{x}/\hbar}\,\mathrm{d}^3q\,. \tag{5.45}$$

In practice, however, the form factor can be measured only over a limited range of momentum transfer $|\boldsymbol{q}|$. The limitation is due to the finite beam energy available and the sharp drop in the cross-section for large momentum transfer. One therefore chooses various parametrisations of $f(r)$, determines the theoretical prediction for $F(\boldsymbol{q}^2)$ and varies the parameters to obtain a best fit between theory and the measured value of $F(\boldsymbol{q}^2)$.

The form factor can be calculated analytically for certain charge distributions described by some simple radial functions $f(r)$. The form factors for some special cases of $f(r)$ are listed in Table 5.1, and are depicted in Fig. 5.7. A charge distribution which drops off gently corresponds to a smooth form factor. The more extended the charge distribution, the stronger the fall-off of the form factor with $\boldsymbol{q}^2$. On the other hand if the object is small, the form factor falls off slowly. In the limit of a point-like target, the form factor approaches unity.

Scattering off an object with a sharp surface generally results in well-defined diffraction maxima and minima. For a homogeneous sphere with radius R, for example, a minimum is found at

$$\frac{|\boldsymbol{q}|\cdot R}{\hbar}\approx 4.5\,. \tag{5.46}$$

The location of the minima thus tells us the size of the scattering nucleus.

In Fig. 5.6 we saw that the minimum in the cross-section of electron scattering off ^{12}C (and thus the minimum in the form factor) is found at $|\boldsymbol{q}|/\hbar\approx 1.8\ \mathrm{fm}^{-1}$. One concludes that the carbon nucleus has a radius $R=4.5\,\hbar/|\boldsymbol{q}|\approx 2.5\,\mathrm{fm}$.

Figure 5.8 shows the result of an experiment comparing the two isotopes ^{40}Ca and ^{48}Ca. This picture is interesting in several respects:

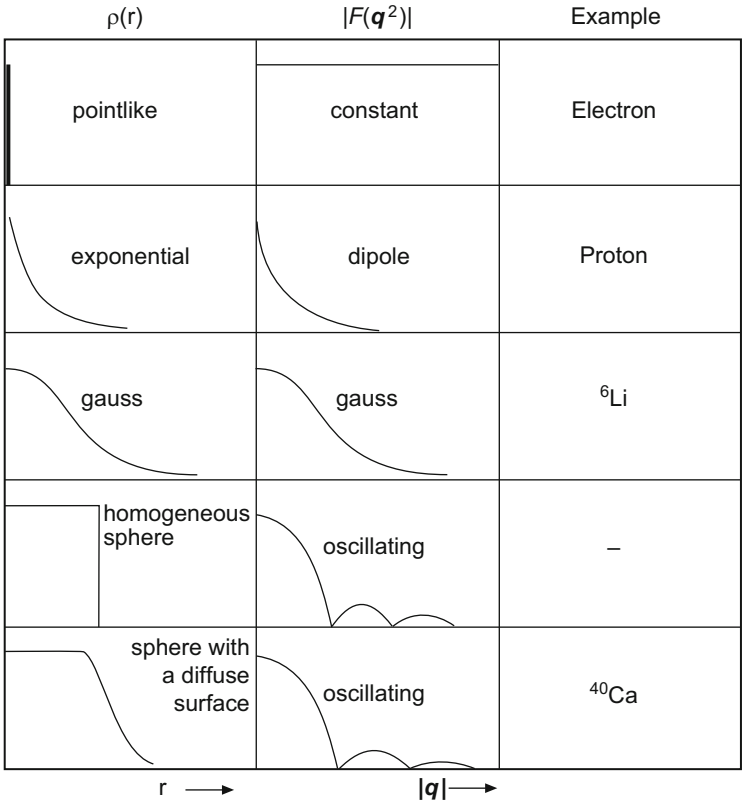

Fig. 5.7 Relation between the radial charge distribution $\varrho(r)$ and the corresponding form factor in Born approximation. A constant form factor corresponds to a point-like charge (e.g., an electron); a dipole form factor to a charge distribution which falls off exponentially (e.g., a proton); a Gaussian form factor to a Gaussian charge distribution (e.g., ^{6}Li nucleus); and an oscillating form factor corresponds to a homogeneous sphere with a more or less sharp edge. All nuclei except for the lightest ones, display an oscillating form factor

– The cross-section was measured over a large range of $|\boldsymbol{q}|$. Within this range, it changes by seven orders of magnitude.[1]
– Not *one* but three minima are visible in the diffraction pattern. This behaviour of the cross-section means that $F(\boldsymbol{q}^2)$ and the charge distribution $\varrho(r)$ can be determined very accurately.
– The minima of ^{48}Ca are shifted to slightly lower values of $|\boldsymbol{q}|$ than those of ^{40}Ca. This shows that ^{48}Ca is larger.

Information about the nuclear radius can be obtained not only from the location of the minima of the form factor, but also from its behaviour for

[1] Even measurements over 12 (!) orders of magnitude have been carried out (cf., e.g., [5]).

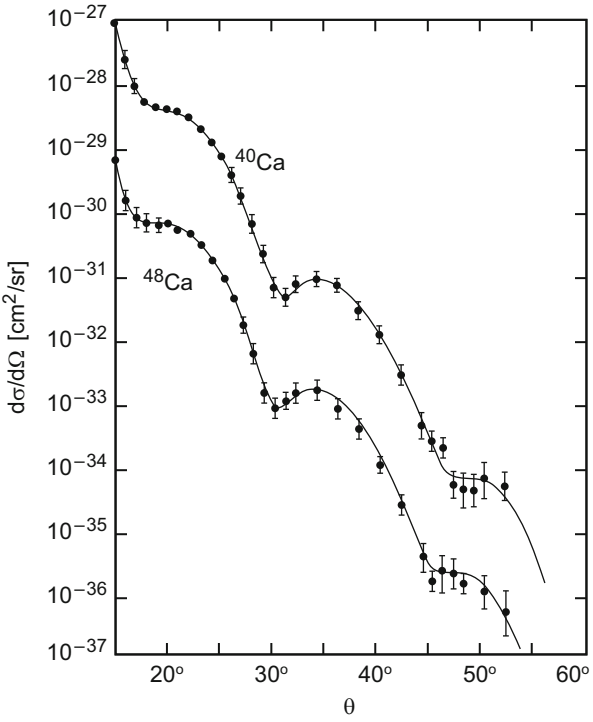

Fig. 5.8 Differential cross-sections for electron scattering off the calcium isotopes ^{40}Ca and ^{48}Ca [1]. For clarity, the cross-sections of ^{40}Ca and ^{48}Ca have been multiplied by factors of 10 and 10^{-1}, respectively. The *solid lines* are the charge distributions obtained from a fit to the data. The location of the minima shows that the radius of ^{48}Ca is larger than that of ^{40}Ca

$\boldsymbol{q}^2 \to 0$. If the wavelength is considerably larger than the nuclear radius R, then

$$\frac{|\boldsymbol{q}| \cdot R}{\hbar} \ll 1 \,, \tag{5.47}$$

and $F(\boldsymbol{q}^2)$ can from (5.42) be expanded in powers of $|\boldsymbol{q}|$:

$$\begin{aligned} F(\boldsymbol{q}^2) &= \int f(\boldsymbol{x}) \sum_{n=0}^{\infty} \frac{1}{n!} \left(\frac{i|\boldsymbol{q}||\boldsymbol{x}| \cos\vartheta}{\hbar} \right)^n \mathrm{d}^3x \qquad \text{with } \vartheta = \sphericalangle(\boldsymbol{x}, \boldsymbol{q}) \\ &= \int_0^{\infty} \int_{-1}^{+1} \int_0^{2\pi} f(r) \left[1 - \frac{1}{2} \left(\frac{|\boldsymbol{q}| r}{\hbar} \right)^2 \cos^2\vartheta + \ldots \right] \mathrm{d}\phi \; \mathrm{d}\cos\vartheta \, r^2 \mathrm{d}r \\ &= 4\pi \int_0^{\infty} f(r)\, r^2 \mathrm{d}r - \frac{1}{6} \frac{\boldsymbol{q}^2}{\hbar^2} 4\pi \int_0^{\infty} f(r)\, r^4 \mathrm{d}r + \ldots \,. \end{aligned} \tag{5.48}$$

Defining the *mean square charge radius* according to the normalisation condition (5.44) by

$$\langle r^2 \rangle = 4\pi \int_0^\infty r^2 \cdot f(r)\, r^2 \mathrm{d}r \,, \tag{5.49}$$

then

$$F(\boldsymbol{q}^2) = 1 - \frac{1}{6} \frac{\boldsymbol{q}^2 \langle r^2 \rangle}{\hbar^2} + \ldots \tag{5.50}$$

Hence it is necessary to measure the form factor $F(\boldsymbol{q}^2)$ down to very small values of $\boldsymbol{q}^2$ in order to determine $\langle r^2 \rangle$. The following equation holds:

$$\langle r^2 \rangle = -6\, \hbar^2 \frac{\mathrm{d}F(\boldsymbol{q}^2)}{\mathrm{d}\boldsymbol{q}^2}\bigg|_{\boldsymbol{q}^2=0} \,. \tag{5.51}$$

Charge distributions of nuclei Many high-precision measurements of this kind have been carried out at different accelerators since the middle of the 1950s. Radial charge distributions $\varrho(r)$ have been determined from the results. The following has been understood:

– Nuclei are not spheres with a sharply defined surface. In their interior, the charge density is nearly constant. At the surface the charge density falls off over a relatively large range. The radial charge distribution can be described to good approximation by a Fermi function with two parameters

$$\varrho(r) = \frac{\varrho(0)}{1 + \mathrm{e}^{(r-c)/a}} \,. \tag{5.52}$$

This is shown in Fig. 5.9 for different nuclei.

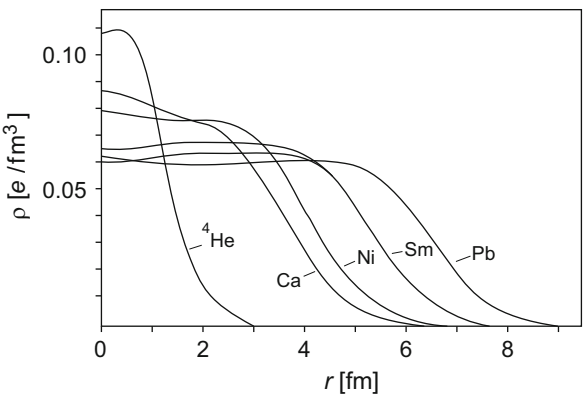

Fig. 5.9 Radial charge distributions of various nuclei. These charge distributions can be approximately described by the Fermi distribution (5.52), i.e., as spheres with diffuse surfaces

– The constant c is the radius at which $\varrho(r)$ has decreased by half. Empirically, for larger nuclei, c and a are measured to be

$$c = 1.07\,\text{fm} \cdot A^{1/3}\,, \qquad a = 0.54\,\text{fm}\,. \tag{5.53}$$

– From this charge density, the mean square radius can be calculated. Approximately, for medium and heavy nuclei

$$\langle r^2 \rangle^{1/2} = r_0 \cdot A^{1/3}\,, \qquad \text{where} \quad r_0 = 0.94\,\text{fm}\,. \tag{5.54}$$

The nucleus is often approximated by a homogeneously charged sphere. The radius R of this sphere is then quoted as the nuclear radius. The following connection exists between this radius and the mean square radius:

$$R^2 = \frac{5}{3}\,\langle r^2 \rangle\,. \tag{5.55}$$

Quantitatively we have

$$R = 1.21 \cdot A^{1/3}\ \text{fm}\,. \tag{5.56}$$

This definition of the radius is used in the mass formula (2.8).

– The surface thickness t is defined as the thickness of the layer over which the charge density drops from 90 % to 10 % of its maximal value

$$t \;=\; r_{(\varrho/\varrho_0=0.1)} - r_{(\varrho/\varrho_0=0.9)}\,. \tag{5.57}$$

Its value is roughly the same for all heavy nuclei, namely

$$t \;=\; 2a \cdot \ln 9 \;\approx\; 2.40\,\text{fm}\,. \tag{5.58}$$

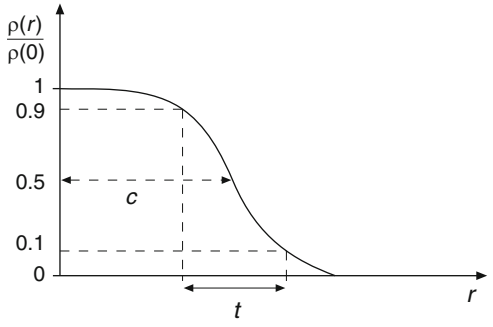

– The charge density $\varrho(0)$ at the centre of the nucleus decreases slightly with increasing mass number. If one takes the presence of the neutrons into account by multiplying by A/Z one finds an almost identical nuclear density in the nuclear interior for nearly all nuclei. For "infinitely large" nuclear matter, it would amount to[2]

$$\varrho_{\mathrm{n}} \approx 0.17 \text{ nucleons/fm}^3 \,. \tag{5.59}$$

This corresponds to a value of $c = 1.12\,\mathrm{fm} \cdot A^{1/3}$ in (5.53).
– Some nuclei deviate from a spherical shape and possess ellipsoidal deformations. In particular, this is found in the lanthanides (the "rare earth" elements). Their exact shape cannot be determined by elastic electron scattering. Only a rather diffuse surface can be observed.
– Light nuclei such as ^{6,7}Li, ^{9}Be, and in particular ^{4}He, are special cases. Here, no constant density plateau is formed in the nuclear interior, and the charge density is approximately Gaussian.

This summary describes only the global shape of nuclear charge distributions. Many details specific to individual nuclei are known, but will not be treated further here [2].

5.5 Inelastic Nuclear Excitations

Above, we have mainly discussed elastic scattering off nuclei. In this case the initial and final state particles are identical. The only energy transferred is recoil energy and the target is not excited to a higher energy level. For fixed scattering angles, the incoming and scattering energies are then uniquely connected by (5.15).

The measured energy spectrum of the scattered electrons, at a fixed scattering angle θ, contains events where the energy transfer is larger than we would expect from recoil. These events correspond to inelastic reactions.

Figure 5.10 shows a high-resolution spectrum of electrons with an initial energy of 495 MeV, scattered off ^{12}C and detected at a scattering angle of 65.4°. The sharp peak at $E' \approx 482$ MeV is due to elastic scattering off the ^{12}C nucleus. Below this energy, excitations of individual nuclear energy levels are clearly seen. The prominent maximum at $E' \approx 463$ MeV is caused by the giant dipole resonance (Sect. 19.2). At even lower scattering energies a broad distribution from quasi-elastic scattering off the nucleons bound in the nucleus (Sect. 6.2) is seen.

[2] This quantity is usually denoted by ϱ_0 in the literature. To avoid any confusion with the charge density we have used the symbol ϱ_{n} here.

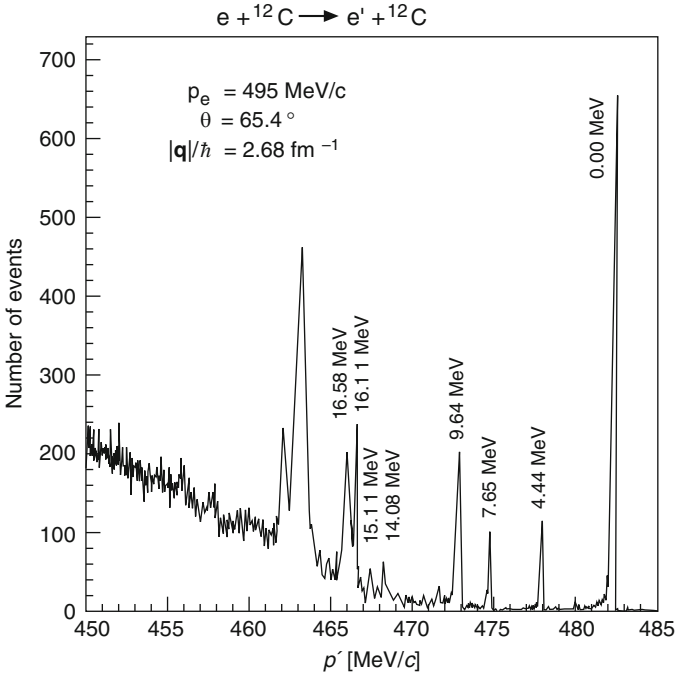

Fig. 5.10 Spectrum of electron scattering off ^{12}C. The sharp peaks correspond to elastic scattering and to the excitation of discrete energy levels in the ^{12}C nucleus by inelastic scattering. The excitation energy of the nucleus is given for each peak. The 495 MeV electrons were accelerated with the linear accelerator MAMI-B in Mainz and were detected using a high-resolution magnetic spectrometer (cf. Fig. 5.5) at a scattering angle of 65.4° (Courtesy of Th. Walcher and G. Rosner, Mainz)

Problems

1. **Kinematics of electromagnetic scattering**
   An electron beam with energy E is elastically scattered off a heavy nucleus.
   (a) Calculate the maximal momentum transfer.
   (b) Calculate the momentum and energy of the backwardly scattered nucleus in this case.
   (c) Obtain the same quantities for the elastic scattering of photons with the same energy (nuclear Compton effect).

2. **Wavelength**
   Fraunhofer diffraction upon a circular disc with diameter D produces a ring shaped diffraction pattern. The first minimum appears at $\theta = 1.22\,\lambda/D$.

Calculate the angular separation of the diffraction minima of α particles with energy $E_{\text{kin}} = 100\,\text{MeV}$ scattered off a ^{56}Fe nucleus. The nucleus should be considered as an impenetrable disc.

3. **Rutherford scattering**
   Alpha particles with $E_{\text{kin}} = 6\,\text{MeV}$ from a radioactive source are scattered off ^{197}Au nuclei. At which scattering angle are deviations from the cross-section (5.16) to be expected?
4. **Form factor**
   Instead of α-particles with $E_{\text{kin}} = 6\,\text{MeV}$ we now consider the scattering of electrons with the same de Broglie wavelength off gold. How large must the kinetic energy of the electrons be? How many maxima and minima will be visible in the angular distribution (cf. Fig. 5.8)?
   Since the recoil is small in this case, we may assume that the kinematical quantities are the same in both the centre-of-mass and laboratory frames.
5. **Elastic scattering of X-rays**
   X-rays are scattered off liquid helium. Which charge carriers in the helium atom are responsible for the scattering? Which of the form factors of Fig. 5.7 corresponds to this scattering off helium?
6. **Compton scattering**
   Compton scattering off bound electrons can be understood in analogy to quasi-elastic and deep-inelastic scattering. Gamma rays from positronium annihilation are scattered off helium atoms (binding energy of the "first" electron: 24 eV). Calculate the angular spread of the Compton electrons that are measured in coincidence with photons that are scattered by $\theta_\gamma = 30°$.

References

1. J.B. Bellicard et al., Phys. Rev. Lett. **19**, 527 (1967)
2. J. Friedrich, N. Vögler, Nucl. Phys. **A373**, 192 (1982)
3. K. Gottfried, V.F. Weisskopf, *Concepts of Particle Physics*, vol. 2 (Clarendon Press, Oxford, 1986)
4. R. Hofstadter, Ann. Rev. Nucl. Sci. **7**, 231 (1957)
5. I. Sick et al., Phys. Lett. **B88**, 245 (1979)